Experimental demonstration of deep frequency modulation interferometry

Katharina-Sophie Isleif,[1,4] **Oliver Gerberding,**[1,3,5] **Thomas S. Schwarze,**[1] **Moritz Mehmet,**[1,2] **Gerhard Heinzel,**[1,2] **and Felipe Guzmán Cervantes**[3]

[1]*Leibniz Universität Hannover, Institute for Gravitational Physics (Albert Einstein Institute), Callinstr. 38, 30167 Hannover, Germany*
[2]*Max Planck Institute for Gravitational Physics, Callinstr. 38, 30167 Hannover, Germany*
[3]*Joint Quantum Institute, University of Maryland, College Park, Maryland 20742, USA & National Institute of Standards & Technology, Gaithersburg, Maryland 20899, USA*
[4]*katharina-sophie.isleif@aei.mpg.de*
[5]*oliver.gerberding@aei.mpg.de*

Abstract: Experiments for space and ground-based gravitational wave detectors often require a large dynamic range interferometric position readout of test masses with $1\,\mathrm{pm}/\sqrt{\mathrm{Hz}}$ precision over long time scales. Heterodyne interferometer schemes that achieve such precisions are available, but they require complex optical set-ups, limiting their scalability for multiple channels. This article presents the first experimental results on deep frequency modulation interferometry, a new technique that combines sinusoidal laser frequency modulation in unequal arm length interferometers with a non-linear fit algorithm. We have tested the technique in a Michelson and a Mach-Zehnder Interferometer topology, respectively, demonstrated continuous phase tracking of a moving mirror and achieved a performance equivalent to a displacement sensitivity of $250\,\mathrm{pm}/\sqrt{\mathrm{Hz}}$ at 1 mHz between the phase measurements of two photodetectors monitoring the same optical signal. By performing time series fitting of the extracted interference signals, we measured that the linearity of the laser frequency modulation is on the order of 2% for the laser source used.

OCIS codes: (120.0120) Instrumentation, measurement, and metrology; (120.2920) Homodyning; (120.3180) Interferometry; (120.5050) Phase measurement; (120.5060) Phase modulation; (140.3518) Lasers, frequency modulated.

References and links

1. K.-S. Isleif, O. Gerberding, S. Köhlenbeck, A. Sutton, B. Sheard, S. Goßler, D. Shaddock, G. Heinzel, and K. Danzmann, "Highspeed multiplexed heterodyne interferometry," Opt. Express **22**, 24689–24696 (2014).
2. A. J. Sutton, O. Gerberding, G. Heinzel, and D. A. Shaddock, "Digitally enhanced homodyne interferometry," Opt. Express **20**, 22195–22207 (2012).
3. D. A. Shaddock, "Digitally enhanced heterodyne interferometry," Opt. Lett. **32**, 3355–3357 (2007).
4. G. de Vine, D. S. Rabeling, B. J. J. Slagmolen, T. T.-Y. Lam, S. Chua, D. M. Wuchenich, D. E. McClelland, and D. A. Shaddock, "Picometer level displacement metrology with digitally enhanced heterodyne interferometry," Opt. Express **17**, 828–837 (2009).
5. G. Heinzel, F. Guzmán Cervantes, A. F. García Marin, J. Kullmann, W. Feng, and K. Danzmann, "Deep phase modulation interferometry," Opt. Express **18**, 19076–19086 (2010).
6. T. S. Schwarze, O. Gerberding, F. G. Cervantes, G. Heinzel, and K. Danzmann, "Advanced phasemeter for deep phase modulation interferometry," Opt. Express **22**, 18214–18223 (2014).
7. K. Danzmann *et al.*, "The Gravitational Universe: Whitepaper for the ESA L2/L3 selection," (2013).

#252465 Received 22 Oct 2015; revised 4 Dec 2015; accepted 7 Dec 2015; published 21 Jan 2016

8. G. Heinzel, V. Wand, A. García, O. Jennrich, C. Braxmaier, D. Robertson, K. Middleton, D. Hoyland, A. Rüdiger, R. Schilling, U. Johann, and K. Danzmann, "The LTP interferometer and phasemeter," Classical Quant. Grav. **21**, p. 581 (2004).
9. M. R. Drinkwater, R. Haagmans, D. Muzi, A. Popescu, R. Floberghagen, M. Kern, and M. Fehringer, "The GOCE gravity mission: ESAs first core Earth explorer," in *Proceedings of the 3rd international GOCE user workshop,* (European Space Agency Noordwijk, The Netherlands, 2006), pp. 6–8.
10. O. Gerberding, "Deep frequency modulation interferometry," Opt. Express **23**, 14753–14762 (2015).
11. J. Zheng, *Optical frequency-modulated continuous-wave (FMCW) interferometry* (Springer Science & Business Media, 2005), Vol. 107 .
12. I. Sakai, R. Youngquist, and G. Parry, "Multiplexing of optical fiber sensors using a frequency-modulated source and gated output," J. Lightwave Technol. **5**, 932–940 (1987).
13. T. Kissinger, T. O. Charrett, and R. P. Tatam, "Range-resolved interferometric signal processing using sinusoidal optical frequency modulation," Opt. Express **23**, 9415–9431 (2015).
14. R. Fleddermann, "Interferometry for a space-based gravitational wave observatory reciprocity of an optical fiber," Ph.D. thesis, Fakultät für Mathematik und Physik der Gottfried Wilhelm Leibniz Universität Hannover (2012).
15. M. Dehne, M. Tröbs, G. Heinzel, and K. Danzmann, "Verification of polarising optics for the LISA optical bench," Opt. Express **20**, 27273–27287 (2012).
16. O. Gerberding *et al.*, "Readout for intersatellite laser interferometry: Measuring low frequency phase fluctuations of high-frequency signals with microradian precision," Rev. Sci. Instrum. **86**, 074501 (2015).

1. Introduction

New interferometer schemes using different phase modulation techniques, like digital interferometry (DI) [1–4] and deep phase modulation (DPM) [5, 6], are currently investigated to simplify the optical part of future experiments in gravitational physics and for metrology experiments. Reduced optical complexity is an attractive improvement considering satellite missions like LISA [7], LISA Pathfinder (LPF) [8] and future geodesy missions [9]. Especially missions that will aim to measure all degrees of freedom of multiple test masses will benefit from such simplifications if they use an optical readout system instead of electrostatic readout, to achieve the sensitivities of $1\,\mathrm{pm}/\sqrt{\mathrm{Hz}}$. The classic heterodyne interferometry used for the 2-test-mass-readout in LPF is too complex to be adapted for future experiments using gradiometers with, for example, six test masses and a full optical readout of all 36 degrees of freedom.

One recently proposed scheme to simplify optical set-ups is the so-called deep frequency modulation (DFM) [10], a type of frequency modulated continuous wave (FMCW) technique [11] that uses strong laser frequency modulations in unequal arm length interferometers in combination with a phase readout based on fitting the complex amplitudes of the modulation harmonics [5]. This fit algorithm is an alternative to established windowing based, multiplexing-capable phase extraction methods [12]. Recent progress in these methods has let to the demonstration of phase measurement sensitivities in the order of $1 \cdot 10^{-4}\,\mathrm{rad}/\sqrt{\mathrm{Hz}}$ above 1 Hz [13]. However, in contrast to DFM these methods require in general much larger frequency modulation amplitudes or optical pathlength differences, because their windowing algorithm extracts the phase only from a part of the interferogram. While DFM does not offer multiplexing without additional components [10], it can tolerate much smaller effective phase modulations since the fit algorithm uses the amplitudes of all relevant harmonics except for the DC component. Test mass readout, especially in satellite missions, greatly benefits from miniaturisation and smaller optical pathlength differences also inherently reduce the laser frequency noise coupling, making DFM in theory the preferred method in this application area.

In this article, we present the first experimental results for the research of this technique. We show the working principle in a Michelson and a Mach-Zehnder Interferometer and we investigate the current performance with optical π-measurements by comparing the noise floor between the two complimentary optical signals generated in the Mach-Zehnder Interferometer. We analyse the noise couplings that are relevant for DFM and based on this we make a prediction about the achievable performances in future implementations.

#252465 Received 22 Oct 2015; revised 4 Dec 2015; accepted 7 Dec 2015; published 21 Jan 2016

2. Deep frequency modulation in a nutshell

We briefly introduce the basics of deep frequency modulation for the sake of completeness. In [10], Gerberding et al., the detailed analysis can be found.

A deep frequency modulation (DFM) of

$$f_{\mathrm{DFM}}(t) = \Delta f \cdot \cos(2\pi f_{\mathrm{m}} t + \psi_{\mathrm{m}}) \tag{1}$$

is applied to the frequency of our laser source. The strength of the modulation is given by the modulation depth Δf, the modulation frequency f_{m}, and the modulation phase ψ_{m} [10]. Considering an interferometer that inserts an optical pathlength difference of τ between the two interfering beams the resulting power on the photodetector is equivalent to an interference with a strong sinusoidal phase modulation [5, 6, 11, 12]

$$P_{\mathrm{out}}(t) = E + E \cdot \kappa \cdot \cos(\varphi + 2\pi\Delta f \tau \cos[2\pi f_{\mathrm{m}} t + \psi_{\mathrm{m}}]), \tag{2}$$

under the assumption that $2\pi f_{\mathrm{m}} \tau \ll 1$, which is valid for modulation frequencies in the order of 1 kHz and the interferometer dimensions used in this article with optical pathlength differences in theirs arms in the order of 10 cm ($\tau < 1$ ns). The equivalent effective phase modulation depth is given by

$$m = 2\pi\Delta f \tau, \tag{3}$$

which linearly depends on the optical pathlength delay τ and on the modulation depth Δf. This allows us to demodulate the signal by applying the deep phase modulation (DPM) readout algorithm, which uses the complex signal amplitudes determined by multiple single-bin Fourier transforms [5]. A sophisticated fit algorithm estimates the four signal parameters, namely the effective modulation depth m, the optical amplitude E, the contrast κ, the interferometric phase φ and the modulation phase ψ_{m}, by comparing the complex amplitudes of the harmonics with the model given by the Bessel functions.

3. Experimental set-up

The experimental set-up is shown in Fig. 1; a fiber-based laser preparation is used, shown in Fig. 1(a). An electro-optical amplitude modulator (EOAM) stabilises the laser amplitude, which fluctuates due to the frequency modulation and due to the inherent noise of the diode laser itself. The stabilised light is split via fiber splitters (FS) and fed into two free beam interferometers. As laser source we use an external cavity laser (TLB 6700 Velocity from Newport) that provides a laser beam with a wavelength of 1550 nm and a laser power of 20 mW maximum. It ensures a continuous, mode-hop-free tuning and can produce strong frequency modulations with peak amplitudes in excess of 10 GHz deviation at frequencies of 1 kHz or higher (range used in this article).

The first of two interferometers, constructed on an aluminium breadboard in the test bed shown in Fig. 1(b), is the Michelson Interferometer (MI). It is used for sinusoidal signal injection at one of its end mirrors. The purpose of this is to test the functionality of the fit algorithm under dynamic disturbances and to simulate phase signals appearing in one of the interferometer arms which should be recovered by the algorithm.

The Mach-Zehnder Interferometer (MZI) is the second interferometer layout that enables us to detect two complementary optical measurements of one interference signal. The photodetector signals P_+ and P_- at both interferometer outputs contain the same optical phase information, but with a phase shift of π due to the recombining beamsplitter. Both interferometers have optical pathlength differences of 94 mm and 137.5 mm for the MI and the MZI, respectively. Applying a frequency modulation amplitude of $\Delta f \approx 3.1$ GHz therefore results in different effective modulation depths (see Eq. (3)) of $m \approx 6.16$ for the MI and of $m \approx 9.01$ for the MZI.

#252465 Received 22 Oct 2015; revised 4 Dec 2015; accepted 7 Dec 2015; published 21 Jan 2016

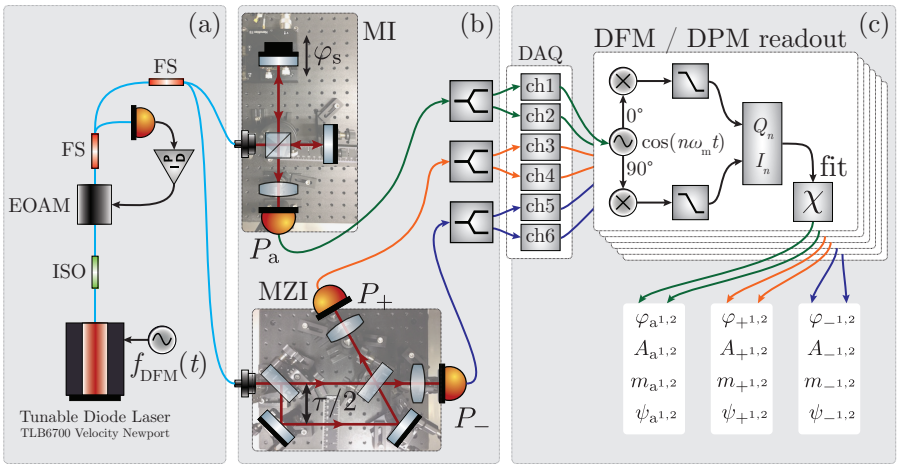

Fig. 1. Sketch of the experimental set-up. The laser preparation shown in (a) is a fiber-based set-up with amplitude stabilisation. The test bed shown in (b) consists of a Michelson Interferometer (MI) and a Mach-Zehnder Interferometer (MZI) which are free beam set-ups. Part (c) shows the data post-processing system using an $IQ-$demodulation and the fit algorithm to extract the phase, amplitude and modulation information.

The interferometers and the laser preparation are operated in air and without any temperature stabilisation other than standard laboratory air conditioning.

The signal detection and data post-processing are shown in Fig. 1(c). The photodetector signals are simultaneously digitised by using a data acquisition (DAQ) card with a sampling rate of 250 kHz per channel. The complex amplitudes of the higher harmonics are determined by using an $IQ-$demodulation scheme that also averages (rectangular window) and decimates the data to a rate of 100 Hz and is implemented in software (LabView). In the last step the frequency domain fit algorithm uses the predicted Bessel function amplitudes to estimate the four signal parameters (C code) [5]. The processing is done in real time on a personal computer. Fig. 3 shows a typical DFM signal (blue dots) that is measured for a modulation frequency of $f_{\mathrm{m}} = 1\,\mathrm{kHz}$ and an effective modulation depth of $m \approx 6.47$ using the MZI layout.

4. Phase measurement performance

The two different interferometer schemes mentioned above allow the investigation of different noise sources by combining the phase measurements of the MI, φ_{a}, and those of the MZI, φ_+ and φ_-, in two different ways.

Electronic noise can be measured by subtracting the two phase readouts generated by electronically splitting one photodetector output and feeding it into two DAQ channels **1** and **2** as it is shown in Fig. 1. The subtraction of the phases from two identical channels theoretically combines to zero:

$$\varphi_{i,\Delta} = \varphi_{i^1} - \varphi_{i^2} \approx 0, \tag{4}$$

with $i = \{\mathrm{a}, +, -\}$, here denoted as zero combination.

An alternative combination is the addition of the phase readouts from two photodetector outputs after the recombining beamsplitter. The combination of the two complementary MZI outputs, here denoted as π-combination, is

$$\varphi_\pi = \varphi_+ + \varphi_- \approx \pi. \tag{5}$$

#252465
Received 22 Oct 2015; revised 4 Dec 2015; accepted 7 Dec 2015; published 21 Jan 2016

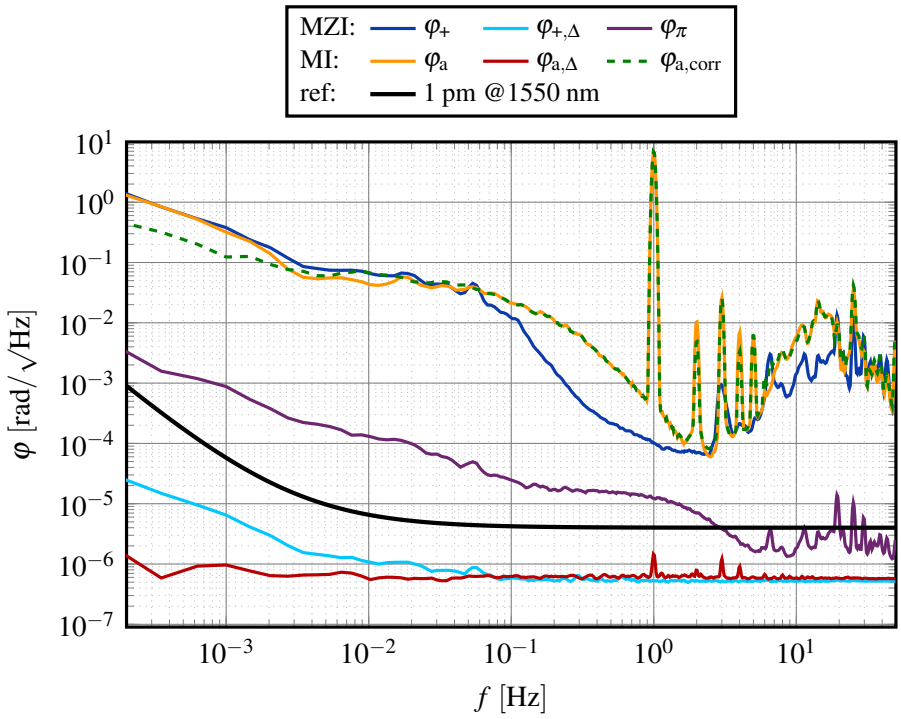

Fig. 2. Spectral densities of the phase determined from the frequency domain fit algorithm using the Bessel function amplitudes [5] with the modulation parameters $f_m = 800\,\text{Hz}$, $m \approx 6.16$ for the Michelson Interferometer (MI) and $m \approx 9.01$ for the Mach-Zehnder Interferometer (MZI). The dark blue line shows the phases φ_+ and φ_- from both interferometric outputs of the MZI. The yellow curve shows the initial phase measurements φ_a from the MI, the green dashed curve shows the corresponding laser frequency noise corrected phase data $\varphi_{a,corr}$. The residuals between two measurements which are electronically split are given by $\varphi_{i,\Delta}$ (red line and light blue line for the MZI and MI). The residuals of the π-combination are given by φ_π (purple line). As reference we also plot the typical 1 pm requirement for the displacement sensitivity aimed at in LISA.

We investigated the phase performance, which is a measure of the expected displacement sensitivity and linearity of the readout from the fit algorithm. To determine the performance at frequencies down to a few mHz1 mHz, the directly measured phases, as well as the signal combinations have been tracked continuously over approximately 12 hours. The results are shown as phase spectral densities in Fig. 2. In the following we will discuss each combination and comment on the relevant noise sources. For each phase and phase spectral density we quote the equivalent, approximate displacement sensitivity in brackets to simplify the comparison with other displacement sensing techniques.

The dark blue and yellow lines represent directly the reconstructed phase outputs for the MZI and MI. The piezo induced length modulation of the MI end mirror at 1 Hz, with an amplitude of approximately 1 rad (250 nm), is clearly visible together with some harmonics. It is unclear if these harmonics are real piezo motion or non-linearity of our readout. DFM is influenced by non-linearities due to finite bandwidth of the analogue front-end and the photodetectors [5], and non-sinusoidal laser frequency modulations [10], which we discus in more detail in the next section. Both interferometer outputs, φ_a and φ_+, show the expected influence of acoustic

#252465 Received 22 Oct 2015; revised 4 Dec 2015; accepted 7 Dec 2015; published 21 Jan 2016

couplings, dominating above 1 Hz and noise increasing to low frequencies. Since we do not have a suitable displacement reference for either interferometer, we at first cannot distinguish if this noise is caused by thermally driven length fluctuations or laser frequency noise. However, one of the fundamental concepts of DFM is the use of a stable reference interferometer to either stabilise the laser frequency noise or to provide a reference measurement of it that can then be subtracted. In our experiment we can consider the MZI as the reference interferometer and the MI as the readout interferometer, within the limits of our thermal and acoustic stabilities. Under this assumptions we have corrected φ_a using the ratio of the two respective modulation depths, which corresponds to the optical pathlength delays and takes into account the different coupling of laser frequency noise. The result is shown as green, dashed line in Fig. 2. We observe a noise reduction only at very low frequencies, but already improving the readout of the MI by about a factor of 2 at 1 mHz and below. Based on this we assume that the low frequency noise was largely dominated by thermal fluctuations and air density changes and not by laser frequency noise. Interferometers that achieve 1 pm/$\sqrt{\text{Hz}}$ level sensitivities below 1 Hz are operated in vacuum with much higher thermal stability and they are additionally constructed from materials with low coefficients of thermal expansion. This explains the discrepancy between our measurements and earlier, more sensitive experiments [14, 15].

However, the earlier introduced combinations, $\varphi_{i,\Delta}$ and φ_π, give valuable insight into the presence of other limiting noise sources. The zero combinations for both interferometers, the light blue and red line in Fig. 2, show a white noise floor of 0.6 µrad/$\sqrt{\text{Hz}}$ (0.15 pm/$\sqrt{\text{Hz}}$) which we assume is caused by additive noise in our signal acquisition, most probably ADC digitisation noise usually present at these levels [16]. Optical noise sources, like shot noise and amplitude noise, are common mode and, hence, do not contribute to this combination. The MI zero combination, $\varphi_{a,\Delta}$, contains a small residual of the 1 Hz mirror modulation and its harmonics. We assume that this coupling is due to small differences in the detection bandwidth of the DAQ system, leading to non-linearities with a resulting dynamic range of about 6 orders of magnitude. The noise in the MZI zero combination, $\varphi_{+,\Delta}$, increases slightly to lower frequencies which cannot be observed in the MI combination. The MZI has a larger effective modulation depth and the photodetector output will be spread more to higher harmonics. These are, in general, more sensitive to temperature induced phase variations in the analogue components and we assume that this behaviour causes the noise increase in the MZI zero combination to lower frequencies [16]. However, both zero combinations showed an improvement of about one order of magnitude in comparison to similar zero measurements demonstrated earlier [6].

Finally, we analysed the π-combination for the MZI, φ_π, plotted as purple line in Fig. 2. The white noise floor of this combination is not clearly visible but it is probably on the same order of magnitude as for the zero combinations. The π-combination is not sensitive to either displacement noise, laser frequency noise or non-sinusoidal frequency modulations because, except for a phase shift of π, both beams contain the same interference. However, this phase shift causes amplitude fluctuations to couple differently in both outputs, making the π-combination sensitive to amplitude noise at the modulation harmonics, as well as shot noise, additive noise in the DAQ and, again, finite detection bandwidth. Above 3 Hz this combination achieves a performance better than 4 µrad/$\sqrt{\text{Hz}}$ (1 pm/$\sqrt{\text{Hz}}$), except for some peaks also visible in the direct interferometer output, φ_+, with a dynamic range of about 3 orders of magnitude. We excluded that this is caused by non-linearities due to finite detection bandwidth by separately measuring the flatness of the photo receivers transfer functions (the receivers have a bandwidth of more than 1 MHz). This leaves some form of unwanted amplitude modulation as the likely cause for this non-linear coupling. Around 1 Hz the π-combination shows a characteristic noise shoulder, which is often caused by small vector coupling [14, 16], leading to a noise floor of 20 µrad/$\sqrt{\text{Hz}}$ (5 pm/$\sqrt{\text{Hz}}$) between 100 mHz and 1 Hz. This small vector coupling is consistent with the noise

#252465 Received 22 Oct 2015; revised 4 Dec 2015; accepted 7 Dec 2015; published 21 Jan 2016

shoulder, the non-linearities at higher frequencies and even the noise increase below 100 mHz which, again shows a dynamic range of about 3 orders of magnitude between the π-combination and φ_+. This leads to a performance of $1\,\mathrm{mrad}/\sqrt{\mathrm{Hz}}$ ($250\,\mathrm{pm}/\sqrt{\mathrm{Hz}}$) at 1 mHz. The amplitude noise, creating the small vector coupling, can either be a classic amplitude fluctuation of the laser light sent into the interferometer or an effective amplitude modulation of the interference caused by ghost beams, stray light or poor polarisation control in the interferometer. The strong frequency modulation is expected to generate some residual amplitude modulation of the laser power at the critical frequencies. While we have implemented a power stabilisation to suppress this somewhat we do not know the effective residual amplitude modulation at the input of the interferometers. Measurements without the power stabilisation did not change the phase performance of the π-combination, leading us to believe that laser induced amplitude modulations are not the limiting factor, however we cannot fully exclude them either. A more probable explanation is poor polarisation control, creating amplitude fluctuations due to polarisation dependent optical properties of the components, or the presence of ghost beams in our set-up due to internal reflections in the beamsplitters caused by non-ideal anti-reflecting coatings [15]. Spurious optical signals that create small vector noise with a dynamic range of about 3 orders of magnitude will have, in a simplified picture, power levels of about 6 orders of magnitude less than the beams of interest. Such contaminations are easily introduced, but these effects can be suppressed in future implementations by using polarisers to extinct unwanted polarisation components and by a detailed stray light analysis and optimisation involving component placement and potentially wedged components to separate ghost beams and the actual interference.

5. Time domain analysis of frequency modulation linearity

A second effect, that can not spoil the performance of φ_π, but the overall readout performance of DFM is the excitation of higher harmonics of the modulation tone in the laser frequency modulation [10, 13]. This can for example be caused by non-linearities in the frequency actuation, realised here by changing the laser cavity length with a piezo crystal. To analyse this in our set-up we utilise another set of fits, which are operating in the time domain. The fits are implemented in Matlab and each one uses a 10 ms long timeseries of our photodiode output of the MZI (here with a slightly different effective modulation depth), sampled at 250 kHz. With the full sampling rate we can include higher modulation harmonics not taken into account by the frequency domain fit used for the phase extraction.

First, we assume a perfectly sinusoidal frequency modulation of the laser and use the following equation, based on Eq. (2), to fit the data:

$$h_1(t) = E + E \cdot \kappa \cdot \cos(\varphi + m\cos[2\pi f_\mathrm{m} t + \psi_\mathrm{m}]). \tag{6}$$

The result of this fit is shown (yellow line), together with the measurement data (black dots), in Fig. 3. It matches the data with a sum of squared errors (SSE) of $227.1\,\mathrm{V}^2$. Under the assumption that the laser was not perfectly modulated at a single frequency but also excited at higher harmonics (here we consider up to 10), Eq. (6) expands to

$$h_{10}(t) = E + E \cdot \kappa \cdot \cos\left(\varphi + \sum_{k=1}^{10} m_k \cos[k \cdot 2\pi f_\mathrm{m} t + \psi_{\mathrm{m},k}]\right). \tag{7}$$

We fitted the same data also with Eq. (7) and the results are shown in Fig. 3 (green line). The extrapolated function $h_{10}(t)$ matches the measured data set better, especially at the turning and reversal points. The improvement is clarified by plotting the residuals of the fit functions to the measured data (red and blue line). The SSE of our fit could be improved by a factor of 25 when using Eq. (7). Regarding the fit output parameters, the values for amplitude E and

#252465 Received 22 Oct 2015; revised 4 Dec 2015; accepted 7 Dec 2015; published 21 Jan 2016

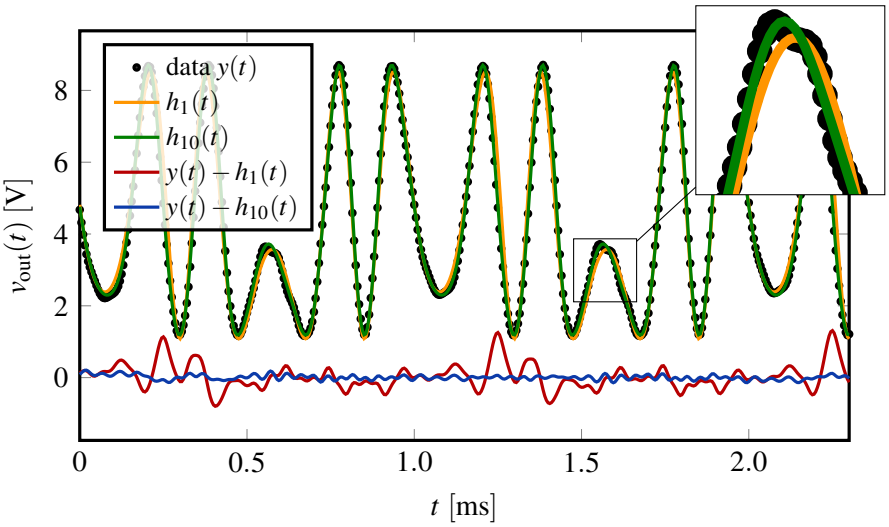

Fig. 3. A typical DFM signal in the time domain of a measured data series for $f_{\mathrm{m}} = 1\,\mathrm{kHz}$ (black dots) and a modulation depth of $m = 6.47$. The function $h_1(t)$, given by Eq. (6) and denoting the theoretical DFM signal, fits the data with a sum of squared errors of SSE = 227.1 V^2. The function $h_{10}(t)$, given by Eq. (7), includes frequency modulations at harmonics of 1 kHz due to the very deep frequency modulation and has an error of SSE = 8.8 V^2. The remaining two curves show the difference of the measured data and the two fit functions.

contrast κ differed by 3%-4% for the different fit functions, but the effective amplitude, given by the product of these values, was identical. The modulation depth for the first harmonics was determined to be $m_1 = 6.47$ for both cases. The first three higher harmonics made the major contribution to the undesired additional frequency modulation with an effective modulation depth of $m_2 = 0.09$, $m_3 = 0.08$ and $m_4 = 0.12$. The maximal contribution of the higher harmonics is about 1.4%, which, if not addressed, will limit the displacement performance in future implementations [10].

6. Conclusion and outlook

This article reports on the implementation of deep frequency modulation interferometry by investigating two interferometer types. A Mach-Zehnder Interferometer was used to validate the functionality and continuous longterm readout given by deep frequency modulation and the sophisticated fit algorithm, operating in the frequency domain, that was originally designed for deep phase modulation. Potential noise sources were identified by comparing two different interferometer types and forming different signal combinations. We have shown that the technique is able to extract actual phase signals injected in one arm of the Michelson Interferometer and that a sensitivity of $0.15\,\mathrm{pm}/\sqrt{\mathrm{Hz}}$ at 1 mHz in a measurement combining two electrical signals to zero is achievable. The π-combination analysed in a Mach-Zehnder Interferometer constellation readily achieved a sensitivity of $250\,\mathrm{pm}/\sqrt{\mathrm{Hz}}$ at 1 mHz without yet applying techniques for stray light suppression or polarisation cleaning [15]. A probably smaller spurious impact on the overall phase performance was given by the excitations of higher harmonics during the very deep frequency modulation injected on the laser source. Using time series fits of our data we were able to quantify this non-linear modulation and thereby to characterise the laser frequency modulation linearity. In future experiments one can either try to actively

#252465 Received 22 Oct 2015; revised 4 Dec 2015; accepted 7 Dec 2015; published 21 Jan 2016

stabilise the modulation or use a more extensive readout scheme to account for them [13]. This could, for example, be an expanded fit algorithm based on the Bessel functions that will include the higher harmonics while running in real-time.

Based on the experience achieved in previous LISA interferometry experiments [15], it is a reasonable assumption that quasi-monolithic, stray light optimised set-ups in vacuum, with higher thermal stability, will enable LISA-like performance levels. Improvements will also be achieved by using polarisation-maintaining fiber components or a free beam laser preparation set-up using a single and clean polarisation orientation. Other effects that remain to be studied in more detail include the laser amplitude stabilisation, to suppress fluctuations at the modulation harmonics, and linearisation schemes of the laser frequency tuning, to ensure sufficiently sinusoidal modulations.

Finally, we can summarise that DFM has been demonstrated to operate with commercially available, conventional equipment, small interferometers and straightforward set-ups, especially in comparison to classic heterodyne techniques. Further development of DFM will surely improve the performance and enable a more elegant optical readout of multiple test masses.

Acknowledgments

The authors would like to thank the DFG Sonderforschungsbereich (SFB) 1128 Relativistic Geodesy and Gravimetry with Quantum Sensors (geo-Q) and Defense Advanced Research Projects Agency (DARPA) and ARO under grant W911NF-14-1-0681 for funding. We thank Jacob M. Taylor for his support to this research and stimulating discussions, Thomas LeBrun for providing laboratory space and equipment and John Kramar for sponsoring the exchange.

Disclaimer: Certain commercial equipment, instruments, or materials are identified in this paper in order to specify the test and measurement procedure adequately. Such identification is not intended to imply recommendation or endorsement by the National Institute of Standards and Technology, nor is it intended to imply that the materials or equipment identified are necessarily the best available for the purpose.

#252465 Received 22 Oct 2015; revised 4 Dec 2015; accepted 7 Dec 2015; published 21 Jan 2016